Hindawi
Advances in Materials Science and Engineering
Volume 2022, Article ID 8454811, 11 pages
https://doi.org/10.1155/2022/8454811

Research Article

Role of Cobalt Doping on the Physical Properties of CdO Nanocrystalline Thin Films for Optoelectronic Applications

Raghavendra Bairy,[1] Ananthakrishna Somayaji,[2] Narasimha Marakala,[2] Udaya Devadiga,[2] M. Rajesh,[3] and John Chuol Wal [4]

[1]*Nitte (Deemed to Be University), NMAM Institute of Technology (NMAMIT), Department of Physics, Udupi 574110, India*
[2]*Nitte (Deemed to Be University), NMAM Institute of Technology (NMAMIT), Department of Mechanical Engineering, Udupi 574110, India*
[3]*Ambedkar Institute of Technology, Department of Mechanical Engineering, Bangalore 560056, India*
[4]*Department of Mechanical Engineering, Gambela University, Gambela, Post Box No. 126, Ethiopia*

Correspondence should be addressed to John Chuol Wal; johnchuol2022@gmu.edu.et

Received 10 September 2022; Accepted 14 October 2022; Published 20 December 2022

Academic Editor: Temel Varol

In the current work, the authors aim to present an insight on the role of cobalt (Co) doping for the structural, morphological, and linear and nonlinear optical (NLO) properties of CdO thin films. The films were prepared using the spray pyrolysis (SP) technique, and the weight % of Co (x) was varied from 0–10. The structural properties of the films were confirmed by the powder X-ray diffraction (P-XRD) studies and are polycrystalline with a cubic structure and a lattice parameter of 0.4658 nm. As Co content in CdO films increases, cluster grain size and porosity decrease significantly, as seen in surface topographic and nanostructural analysis. Through the Burstein–Moss shift, the optical band gap "Eg" in Co: CdO film decreases from 2.52 to 2.05 eV with the increase in Co-doping. To study the NLO parameters, open aperture (OA) and closed aperture (CA) Z-scan measurements were performed using the diode-pumped solid-state continuous wave laser excitation (532 nm), and with the increased Co-content, the NLO parameters—nonlinear absorption coefficient (β~10^{-3} cm/W), nonlinear refractive index ($n_2 \sim 10^{-8}$ cm^2/W), and the 3rd-order NLO susceptibility ($\chi^{(3)} \sim 10^{-7}$ to 10^{-6} e.s.u.) values were determined and found to be enhanced. The maximum NLO parameters achieved in the present study with increasing Co concentration on CdO nanostructures prepared by the SP method are found to be the highest among the reported values and suggest that processed films are a capable material for optoelectronic sensor applications.

1. Introduction

Transparent conducting oxides (TCOs) are widely used in optoelectronic devices such as flat panel displays, organic light emitting diodes, photovoltaics, heat reflectors, and energy-efficient windows because they are electrically conductive and optically transparent [1–3]. CdO is a promising transparent conducting oxide (TCO) due to its high electrical conductivity ($<10^3\ \Omega^{-1}\cdot$cm^{-1}) and its direct band gap of 2.2 eV. It also has a nonstoichiometric composition, which is because of the presence of cadmium interstitial oxygen vacancies acting as donors [4]. The introduction of cobalt, which is a transition magnetic metal element, to CdO led to astonishing optical, electrical, and magnetic properties. This is mainly because of the interaction between the band electrons and the cobalt ion within the CdO lattice.

A review of the literature on pure and doped CdO films reveals a huge array of fabrication studies. In addition to vacuum evaporation, successive ionic layer adsorption and reaction technique, sol-gel technique, magnetron sputter, organic chemical vapour deposition system, chemical spray pyrolysis, chemical bath coating, successive ionic layer adsorption and reaction technique, pulsed laser deposition, and others, thin films deposition methods have been

reported to produce undoped and metal-doped CdO thin films. A key consideration for selecting appropriate contributing materials is the ionic radius [5]. (Co^{2+}) is projected to be the optimal doping candidate for CdO films because it substitutes the Cd^{2+} sites in the lattice and contributes electrons to serve as charge carriers [6]. Structural, optical, and NLO properties of CdO film could be controlled with Co-doping because the ionic radius of Co being smaller than that of cadmium ions [7].

From the literature review, we found Al: CdO films and N: CdO films deposited by the SP technique withlinear and nonlinear optical properties [8, 9]. As a result, we attempted to prepare and study the $Cd_{1-x}Co_xO$ films using this versatile technique. Furthermore, dilute concentration was chosen because we need homogeneous solutions in the SP technique so that during spray, chemical reactions take place in proportion, resulting in a homogeneous thin film in its entire volume. So far, there has been no discussion of the detailed report on NLO studies of $Cd_{1-x}Co_xO$ films. The present study aimed to prepare pure and $Cd_{1-x}Co_xO$ thin films using the SP technique by varying the various contents of Co from 0 to 10 wt. % by volume and focused more on the enhancement of the structural, linear, and 3rd-order NLO properties by the *Z*-scan technique for optoelectronic device applications.

2. Experimental

2.1. Undoped and Co-Doped CdO Thin Films Preparation. Thin films of $Cd_{1-x}Co_xO$ (with "x" wt.% Co of 0, 0.01, 0.05, and 0.1) were fabricated on glass substrates by the SP technique. To remove contaminants from the surface of the glass substrates, they were dipped in a chromic oxide solution for 24 hours. These were then cleaned with detergent and acetone and rinsed. To fabricate the undoped CdO thin films, the cadium acetate dehydrate of 2.66 g is dissolved in 100 ml of double-distilled water to obtain the precursor standard solution of 0.1 M cadmium acetate. The thin films of CdO with a different doping concentration of Co are fabricated by mixing the proper ratio by volume of cadmium acetate dehydrate and cobalt chloride (0.1 M) solutions, which are properly mixed and loaded to an SP instrument and sprayed on a well-cleaned glass substrate. Nozzle to spray distance was kept at 15 cm, and the spray interval was 3 mins. The total duration of film coating was adjusted to get a film thickness of ±450 nm. During the deposition, the substrate temperature was preserved at 573 K (±2%). The reaction for the formation of $Cd_{1-x}Co_xO$ films can be written as

$$Cd(CH_3COO)_2 \cdot 2H_2O + CoCl_2 \xrightarrow[\text{Decompose}]{300^{\circ}C} CdCoO\downarrow + CO_2\uparrow + CH_4 + \text{Steam}. \quad (1)$$

The thickness of the as-prepared thin films was determined using SEM cross-sectional analysis and also confirmed using the gravimetric method, and it ranged from 500 nm–530 nm. The Carl Zeiss FESEM instrument was used to examine the surface morphology of the grown thin films. By using a powder X-ray diffractometer (Rigaku Miniflex 600) and nickel-filtered copper Ka radiation with a wavelength of 1.5418 Å, the structural characterization of the films was carried out. Using the double-beam spectrophotometer (Shimadzu 3600 UV-Viz), the absorbance and transmittance of the prepared thin films were measured in the spectral range of 400–800 nm. The NLO properties were determined using the *Z*-scan technique by the diode-pumped solid-state CW laser (200 mw) at an excitation wavelength of 532 nm.

3. Results and Discussions

3.1. Structural Properties. Figure 1 reveals XRD patterns of thin films of $Cd_{1-x}Co_xO$ with various Co concentrations (0, 1, 5, and 10 wt. %). The patterns in XRD confirm the nature and correspond to the planes (1 1 1), (2 0 0), and (2 2 0) that fit with the pure CdO polycrystalline structure. The P-XRD patterns show that the pure film has a strong (1 1 1) superior orientation, which increases as the concentration of Co-doping increases. The factor f (h, k, and l) values were determined using the method proposed by Jin et al. [10]. As the concentration of Co increases, the 2θ-values of the peaks (1 1 1) and (2 0 0) change to a lower 2θ-value, favouring an expansion in the lattice volumes of the doped films. The peaks on the graph plotted are in the planes of (111) and (200), which are the major peaks, whereas, the (220) and (311) planes are minor peaks. The peaks obtained from the P-XRD graph, which match JCPDS card no. 05-0640, confirm the cubic structure of the samples. By increasing the Co-doping from 1% to 10 wt. %, the broadening of the peaks along the preferential directions of the (111) and (200) planes can be observed. The crystallite size (D_{avg}) was calculated using the Scherer equation (1) [11].

$$\frac{0.9\lambda}{\beta \cos\theta}, \quad (2)$$

where k is the Scherer's constant and is equal to 0.9 for spherical crystals (wurtzite/cubic), β is the full width at half maximum (FWHM), θ is the Bragg's angle, which is given in radians, and the calculated values are shown in Table 1. The diffraction patterns were indexed into a polycrystalline lattice, and the lattice parameters were calculated using the following formula:

$$n\lambda = 2d \sin\theta. \quad (3)$$

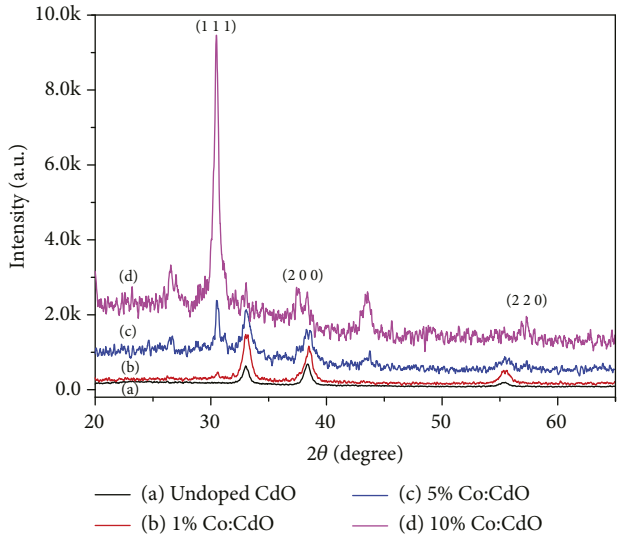

Figure 1: Powder X-ray diffractograms, as a function of Co-doping level on CdO thin films.

The lattice constant (a) was determined using the following formula [12]:

$$d_{hkl} = \frac{a}{\sqrt{h^2 + k^2 + l^2}}. \quad (4)$$

It is observed that with an increase in the lattice-parameter values excessive accumulation of Co-doping as predicted. The enhancement in lattice parameter values may be due to the strain caused by the replacement of Co^{2+} in the host CdO lattice, which has an ionic radius of 1.2 Å, i.e., more than that of Cd^{2+} (0.97 Å). Also, c/a values remained constant; indicating Co-doping has no effect on the ultimate crystal structure of CdO. Microstructural parameters such as strain (ε), density, and density of dislocation (d) were determined using the following formula [13]:

$$\delta = \frac{n}{D^2}, \quad (5)$$

and

$$\varepsilon = \frac{\beta \operatorname{Cos}\theta}{4}. \quad (6)$$

The decreased ε and δ values obtained strongly support the Co-doping on CdO nanostructures. The value of "D_{avg}" was found to be in the range of 10 nm–20 nm, which indicates the films are composed of nanocrystallites, and the variations are shown in Figure 2.

The value of "d" of the undoped CdO film was found to be $a = 0.4658$ nm, which is a bit less than the reported value of $a = 0.4694$ nm, which is due to the lattice contraction or to the presence of O vacancies [14]. The lattice constant "a" remains nearly constant for 1% (0.4566 nm) of cobalt (Co) doping in CdO crystal, but for 5% (0.4578 nm) and 10 wt. % (0.4652 nm) cobalt (Co) doping, it increases. This is due to the fact that the covalent atomic radius of the Co^{2+} ion (0.160 nm) is greater than that of the Cd^{2+} (0.149 nm). The calculated dislocation δ is increased for the (111) and (200) planes. By raising the dopant concentration, this supports the hypothesis that the number of crystallographic defects per unit area varies asymmetrically.

3.2. Surface Morphological Studies. The FESEM images of undoped and Co-doped CdO thin films are displayed in Figure 3. The micrographs show a distinct reduction in grain size and a shift in the growth direction of CdO films as Co concentrations increase.

As a consequence, the FESEM characteristics support the powder X-ray findings that, as Co-doping concentration rises, crystallite size reduces and particle growth direction changes. Similar outcomes for MOCVD-prepared Ga-doped CdO films have been reported [15].

3.3. EDAX for Compositional Analysis. The EDAX spectra show the elementary compositions obtained from all the films and are nearly equal to the fraction of the theoretical volume, which indicates the formation of the CdO structure shown in Figures 4(a) and 4(b) and confirms the existence of Cd, O, and Co components in the film. The O/Co ratios were reduced, indicating that the films lacked a little O or had too much Co. The technique for growing CdO films has also been enhanced. Table 2 depicts the chemical composition of undoped and Co-doped CdO nanostructured thin films.

3.4. Optical Properties. The absorbance spectra of the CdO:Co thin films are shown in Figure 5(a). The spectra for all of the films have the same shape, and the absorbency of CdO films coated with 1, 5, and 10 wt. % Co-doping concentrations is higher than that of the undoped film. The variation can be correlated with the Co-doping concentration in the films. It is well known that the result of increased doping is an increase in the number of atoms, and thus more states are present. As a result, absorption is increased [16] for the energy to be absorbed.

In the inset of Figure 5(b), the transmittance spectra of Co:CdO nanostructures are shown. In the visible region, all of the films have an average transparency of 90%. It is discovered that CdO films coated with 1, 5, and 10 wt.% of Co-doping concentration exhibit lower transparency, while films with undoped CdO films exhibit higher transparency when compared to the doped film. This could be attributed to higher thickness values, which increase light scattering losses [17].

The absorption coefficient (α) of all thin films is calculated using the transmission, reflection, and thickness measurements obtained using the equation [18] and is found to be on the order of $10^4\,\mathrm{cm}^{-1}$as follows:

$$\alpha = \frac{2.303\,\mathrm{A}}{t}. \quad (7)$$

The absorption index (k) was calculated using the formula $k = \alpha\lambda/4\pi$. The larger k value (Figure 5(c)) indicate the defect in the film. Using the value of reflectance (R) and α, the refractive index (Figure 5(d)) was calculated as [19]

Table 1: Powder X-ray diffractogram parameters for the $Cd_{1-x}Co_xO$ thin films.

Sample (%)	(h k l) value	2θ (deg)	FWHM (β)	$d_{h\,k\,l}$ (Å)	Lattice constant (Å)	Crystallite size "D" (nm)	Internal strain "ε"	Dislocation density "δ" $\times 10^{15}$ (W)
CdO	(1 1 1)	33.01	0.8053	2.71	4.6959	17.95	0.67	3.10
	(2 0 0)	38.37	0.7269	2.34	4.6864	20.18	0.52	2.45
$Cd_{0.99}Co_{0.01}O$	(1 1 1)	33.04	0.8793	2.70	4.6902	16.44	0.74	3.69
	(2 0 0)	38.47	0.9065	2.33	4.6750	16.19	0.64	3.81
$Cd_{0.95}Co_{0.05}O$	(1 1 1)	33.07	0.8962	2.70	4.6860	16.13	0.75	3.84
	(2 0 0)	38.56	0.9458	2.33	4.6638	15.52	0.67	4.15
$Cd_{0.90}Co_{0.10}O$	(1 1 1)	33.09	0.9154	2.70	4.6836	15.79	0.77	4.01
	(2 0 0)	38.71	1.4345	2.32	4.6468	10.24	1.02	9.53

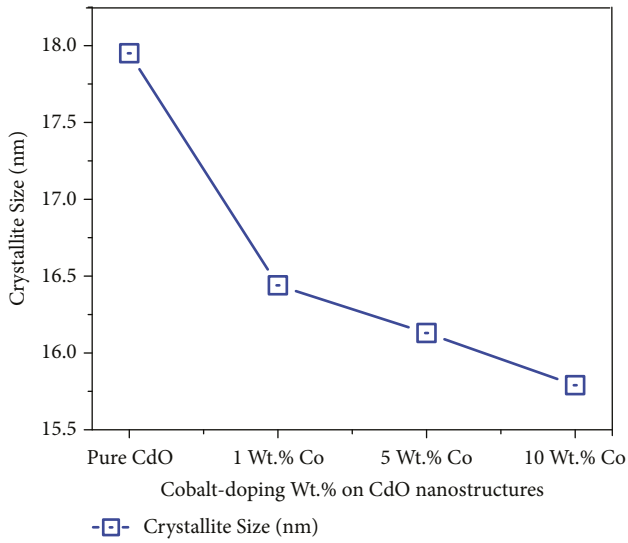

Figure 2: Variations of "D_{avg}" with Co-doping for CdO thin films.

$$n = \frac{(1+R)}{(1-R)} + \sqrt{\frac{4R}{(1-R)^2} - k^2}, \tag{8}$$

where "t" is the thickness of the films. The absorption coefficient is proportional to the energy of the incident photon ($h\nu$) as [20]

$$\alpha h\nu = A\left(h\nu - E_g\right)^{0.5}. \tag{9}$$

A plot of $(\alpha h\nu)^2$ vs. E ($h\nu$ in eV allows an estimate of the "Eg" and is shown in Figure 5(e). The Eg value of the undoped CdO film is 2.52 eV, which decreases to 2.05 eV for the film fabricated with 10 wt. % of Co-doping. Similar band-bowing results have previously been reported for Al-doped CdO films prepared using the SP technique [21]. This may be explained by their greater thickness and stoichiometry, as the decrease in band gap with Co content can also be explained by sp-d exchange interactions between the band electrons in CdO and the localized d electrons of the Co^{2+} [22]. The Burstein–Moss (BM) effect [23], in which the dopant Co-2p ions cause an enhancement in free carrier concentration, which lifts the E_F up to the CB and results in a decrease in Eg value, can be used to explain the red shift in the Eg value of the films coated with 10 wt. % Co-doping concentration.

3.5. Third Order Nonlinear Optical Studies. Semiconducting materials with nonlinear operations are used in valuable applications in the modern technological world of laser devices. The NLO properties of thin films are caused by nonlinear polarisation, which occurs when the material is subjected to a strong electric field. Even in weak NLO materials, the laser is a high-intensity source powerful enough to cause NLO mechanisms such as 2nd and 3rd-order NLO effects. The charge distribution changes as a result of the strong electric fields, resulting in a net dipole moment. The NLO phenomenon is important in a variety of devices, including electro-optic modulators and frequency converters [24–35]. The induced dipole moment per unit volume, also known as electrical polarisation (P), plays an important role in the NLO phenomenon. In a nonlinear medium, the polarisation of light is given by (P_{NL}) [26]

$$P = X^{(1)} \cdot E + P_{NL}. \tag{10}$$

In the abovementioned equation, $P_{NL} = \chi^{(2)}E + \chi^{(3)}$ E. P is the polarizability, $\chi^{(1)}$ depicts the conventional linear response, $\chi^{(2)}$ represents the 2nd, and $\chi^{(3)}$ is the 3rd-order NLO susceptibilities, respectively. NLO materials are extremely important in photonic devices. The open aperture (OA) and closed aperture (CA) Z-scan methods were performed with an $I_o \approx$ of 8.48×10^7 W/m^2 (input intensity) and are illustrated in Figure 6.

The Z-scan technique established and developed by Bahae et al. [27] is an efficient tool for probing the third-order NLO that dwells up in the sample when the incident beam of light is of sufficient intensity and frequency. The samples were placed at the focus $Z = 0^{th}$ position, and the output intensity of the transmitted beam was successively recorded using the far field photo-detector. The beam profile and sample thickness are the most important factors in this approach. In order to maintain a continuous beam profile, the thickness of the sample should always be kept lower than the Rayleigh range. The pure and doped CdO films possess good NLO characteristics. As a result, it appears necessary and justifiable to investigate the NLO properties of Co: CdO films in terms of laser applications. The OA measurements for thin films of $Cd_{1-x}Co_xO$ are shown in Figure 7. When the input intensity (I_{in}) is exceptionally large, there is a substantial increase in the likelihood that a material will absorb more than one photon before going into the ground state. There are many different types of NLA processes. The RSA effect is caused by the fact that ground-state linear absorption dominates excited-state absorption (ESA) in the sample.

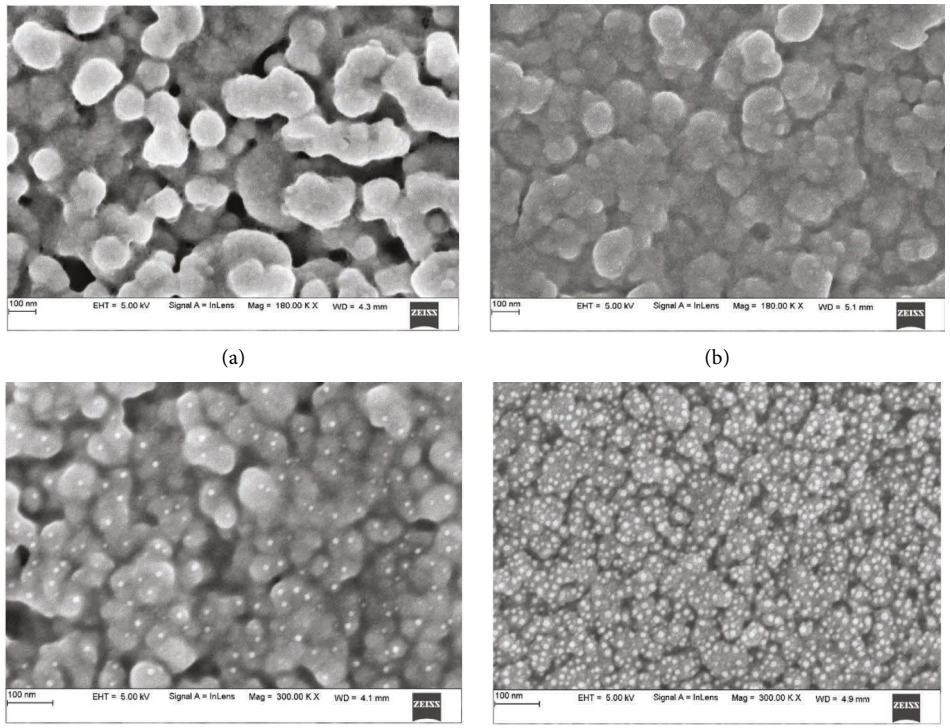

(a) (b)

(c) (d)

Figure 3: FESEM images of (a) pure CdO, (b) 1 wt. % Co, (c) 5 wt. % Co, and (d) 10 wt. % Co of $Cd_{1-x}Co_xO$ nanostructures.

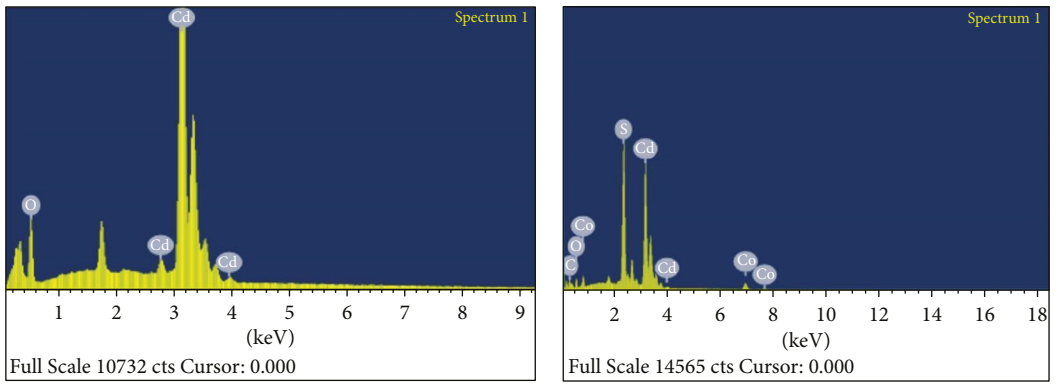

(a) (b)

Figure 4: EDAX images of(a) undoped CdO and (b) 10 Wt. % Co-doped CdO thin films.

Table 2: Chemical composition for undoped and Co-doped CdO thin films.

Material	Element					
	Wt (%)			At (%)		
	Cd (2%)	Co (±2%)	O (±2%)	Cd (±2%)	Co (±2%)	O (±2%)
Undoped CdO	89.20	0	10.80	51.55	0	48.45
1 wt. % of Co	88.35	01.15	11.50	48.35	01.10	51.55
5 wt. % of Co	85.55	04.33	10.12	45.55	05.40	49.05
10 wt. % of Co	79.63	10.15	10.22	38.20	10.65	51.15

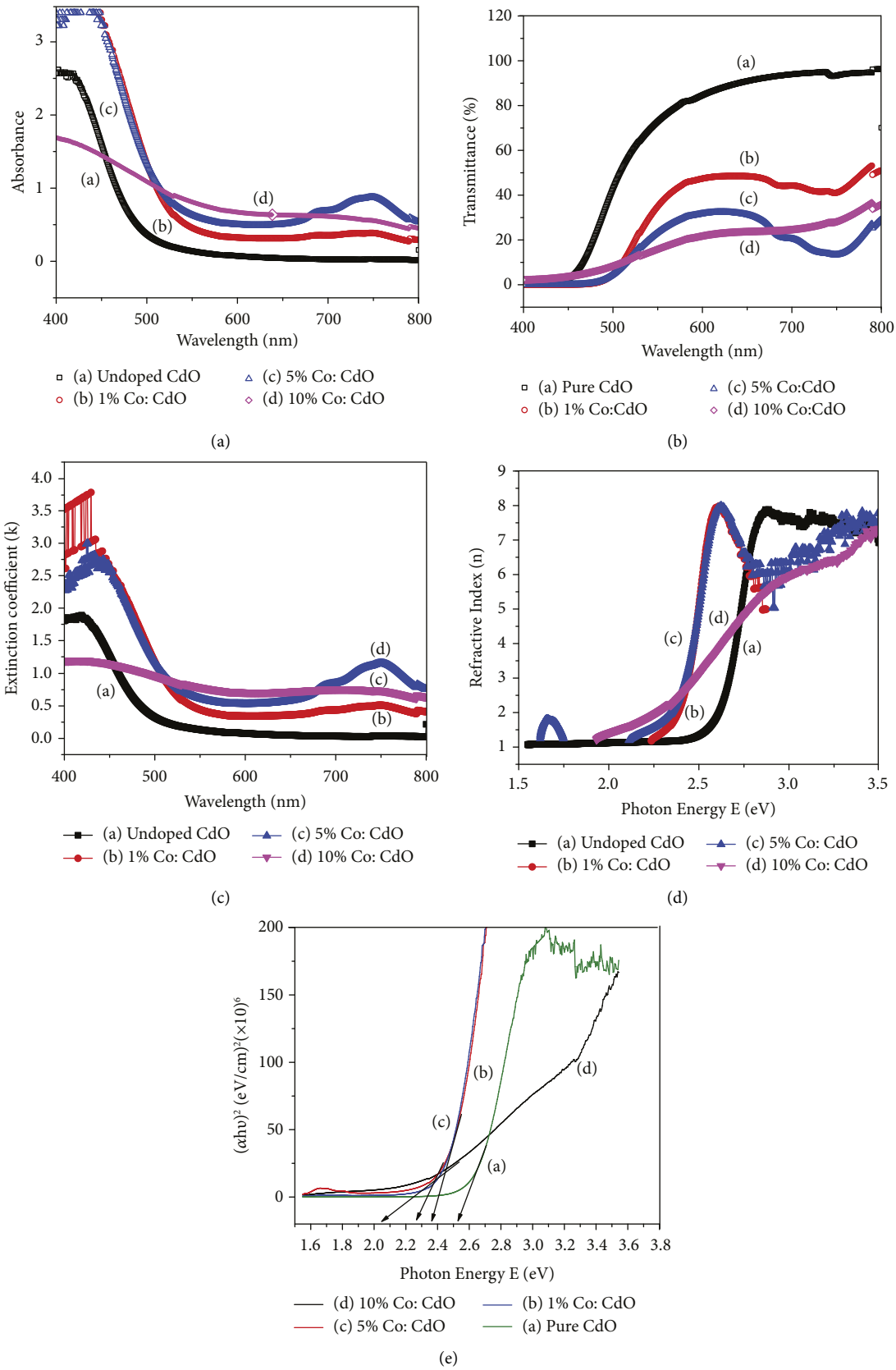

FIGURE 5: (a) absorbance and (b) transmittance with wavelength (nm) for $Cd_{1-x}Co_xO$ thin films. (c) Extinction coefficient with wavelength (nm) and (d) refractive index vs. photon energy of Co-doped CdO films. (e) Eg for the $Cd_{1-x}Co_xO$ thin films.

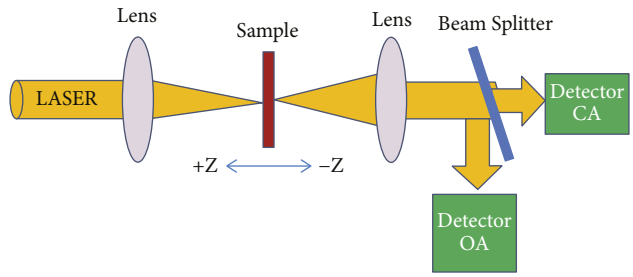

Figure 6: Investigational Z-scan setup.

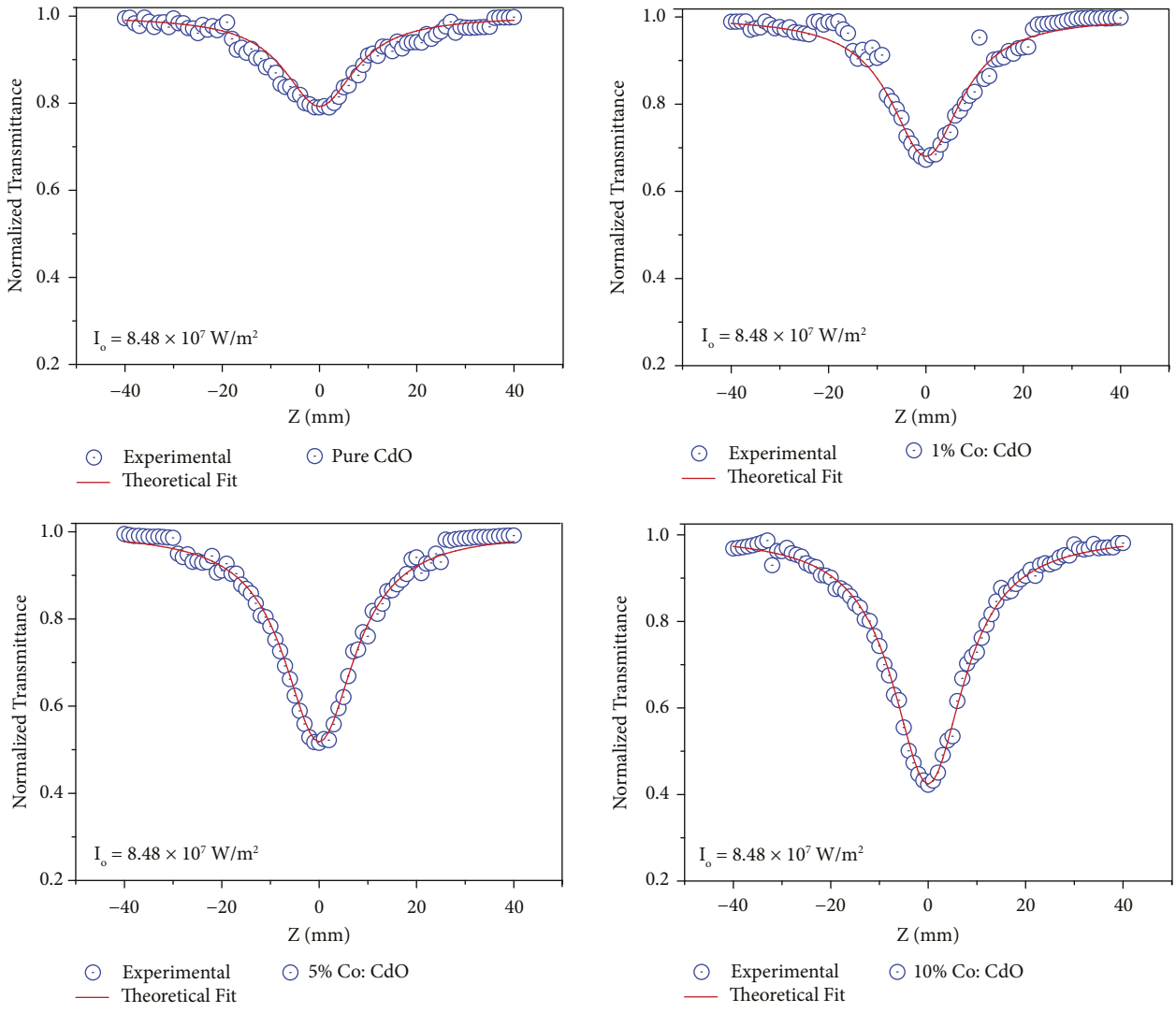

Figure 7: Z-scan OA traces for $Cd_{1-x}Co_xO$ films.

3.5.1. Nonlinear Optical Absorption. The absorption ratio (β) improves with optical intensity in NLA, and the enhancement of (β) occurs in RSA. These phenomena appear optically as reduced (SA) or enhanced (RS) absorption [28]. The transmission curve reveals a standardised transmittance valley with reference to the $Z = 0$ focus, where there is low transmission, indicating that the samples comprise induced absorption. By fitting the standard transmission data to the OA formula, the values of may be obtained from the experimental OA Z-scan findings using the following equation [29]:

$$T(z)_{open} = 1 - \frac{\beta I_o L_{eff}}{2\sqrt{2}\left[1 + Z^2/Z_o^2\right]}. \quad (11)$$

Table 3: NLO parameters of $Cd_{1-x}Co_xO$ thin films.

Composition of Co (X)	NLA	NRI ($\mathbf{n}_2$) $\times 10^{-8}$ (cm^2/W)	Real part of NLO susceptibility ($\chi^{(3)}$ R) $\times 10^{-7}$ (esu)	Imaginary part of NLO susceptibility $\times 10^{-7}$ ($\chi^{(3)}$ img) esu	Third order NLO susceptibility (χ^3)
Wt.%	Coefficient (β) $\times 10^{-3}$ (cm/W)	5.33	6.78	Davg	(Esu)
Pure CdO	0.92	−1.35	7.53	3.19	7.62×10^{-7}
1% Co	1.35	−1.48	8.06	3.26	8.32×10^{-7}
5% Co	3.64	−1.68	9.12	4.46	9.36×10^{-7}
10% Co	6.18	−1.86	9.85	5.62	1.42×10^{-6}

In the abovementioned equation, $L_{eff} = [1 - \exp^{-\alpha_o' d}/2\,\alpha_o']$ is the sample effective thickness and $Z_o = \pi\omega_o^2/\lambda$ is a beam-waist.

The normalised transmittance valley deepens, with a significant upgrade in β values observed with Co-doping concentrations in CdO. The TPA mechanism occurred in CdO: Co films because the energy "E" was less than the "Eg" but greater than Eg/2. Thus, electrons are absorbed and stimulated at the higher energy levels before they reach the ground state [30]. As the Co-doping was increased, there was a noticeable improvement in the RSA mechanism and the relative worth of the produced thin films.

In the current scenario, as a source of excitation, CW lasers have been used, and the source of nonlinearity can also be thermal, with the sample also acting as a thermal lens [31]. Furthermore, the films found current leakage and nano-structural features that support the lattice defects. Table 3 shows the calculated β values of the $Cd_{1-x}Co_xO$ nanostructures.

3.5.2. Nonlinear Refractive Index. The CA Z-scan technique was used to calculate the n_2 and $\chi^{(3)}$ of the synthesised samples. In this configuration, an aperture after the sample limits the transmitted light to the detector. Nonlinear optical materials' self-focusing or self-defocusing effects cause changes in the intensity of light received by the detector. The NLR index of samples varies as the sample scans the z-axis and the beam transmittance changes. The Z-scan CA experimental data show a postfocal peak followed by a prefocal valley, indicating a negative sign of n_2 due to the samples' self-defocusing nature [32]. The experimental results (scattered pattern) agree well with the theoretical results (solid line) suggested by Sheik-Bahae. The functions fitted to the experimental CA data are displayed in Figure 8. The increased polarizabilities and n_2 are due to the atoms' larger atomic radius [33]. From the CA, the parameters have been calculated by the following standard formulae:

$$T(Z) = 1 - \frac{4\,\Delta\phi_o X}{\left(X^2 + 1\right)\left(X^2 + 9\right)}, \tag{12}$$

$x = z/z_o$ and $\Delta\phi_o = Kn_2 I_o L_{eff}$, the value of n_2 is calculated.

The inclusion of Co-material in the fabricated CdO: Co films raises the linear and nonlinear refractive indexes. The increasing behaviour of the Co-doping concentration can be explainedin terms of enhanced crystallinity. Because Co^{2+} ions have large polarizability and very little cat-ionic field intensity, the value of n_2 in CdO can be amplified by the significant polarizability produced by Co-ions. The structural properties and surface morphology are important factors in light-intensity scattering to achieve the expected NLO effect [34]. In fact, the theoretical and experimental normalised transmittances are very close. This results in a thermal lens and severe phase distortion of the propagating beam [35]. In summary, thermal nonlinearity causes the defocusing effect. It is worth noting that particle size influences optical nonlinearity. In the synthesised samples, there is a clear increasing trend for nonlinearity with particle size as the Co concentration in CdO increases. This observation is consistent with what has been reported by others [36].

The following equations are used to calculate the $\chi^{(3)}$ (eeal and imaginary) of $Cd_{1-x}Co_xO$ deposited thin films [37]:

$$\begin{aligned} \mathrm{Re}\,\chi^{(3)} &= 2C\,\varepsilon_o n_2 n_o^2 \\ \mathrm{Im}\,\chi^{(3)} &= \frac{C\,\varepsilon_o \beta\,\lambda\, n_o^2}{2\pi} \\ \left|\chi^{(3)}\right| &= \left|Re\chi^{(3)} + iIm\chi^{(3)}\right| \end{aligned} \tag{13}$$

All nonlinear optical parameters of the $Cd_{1-x}Co_xO$ nanoparticles are given in Table 3. The structural symmetry of the material is directly related to the higher order $\chi^{(3)}$ of the $Cd_{1-x}Co_xO$ deposited thin films (Table 4). Variations of NLO susceptibility (e.s.u.) with crystallite size (nm) for the different doping concentrations of Co in the $Cd_{1-x}Co_xO$ thin films are shown in Figure 9. The improved NLO behaviour of the synthesised samples is associated with improved polarizability and an enlarged carrier concentration for higher Co-content [38].

The NLO properties of synthesised samples can be directly caused by their structural properties [39]. Actually, the much higher polarizability observed for Co-doped CdO samples compared to pristine CdO samples resulted from the higher atomic mass of the substituted Co ions for the Cd ones. Table 4 shows the current and some of the reported values of a few metal sulphide/oxide films for β, n_2 and $\chi^{(3)}$ [40, 41] and [42]. Nevertheless, for optical switching applications, the actual potency of these materials is heavily dependent on n_2.

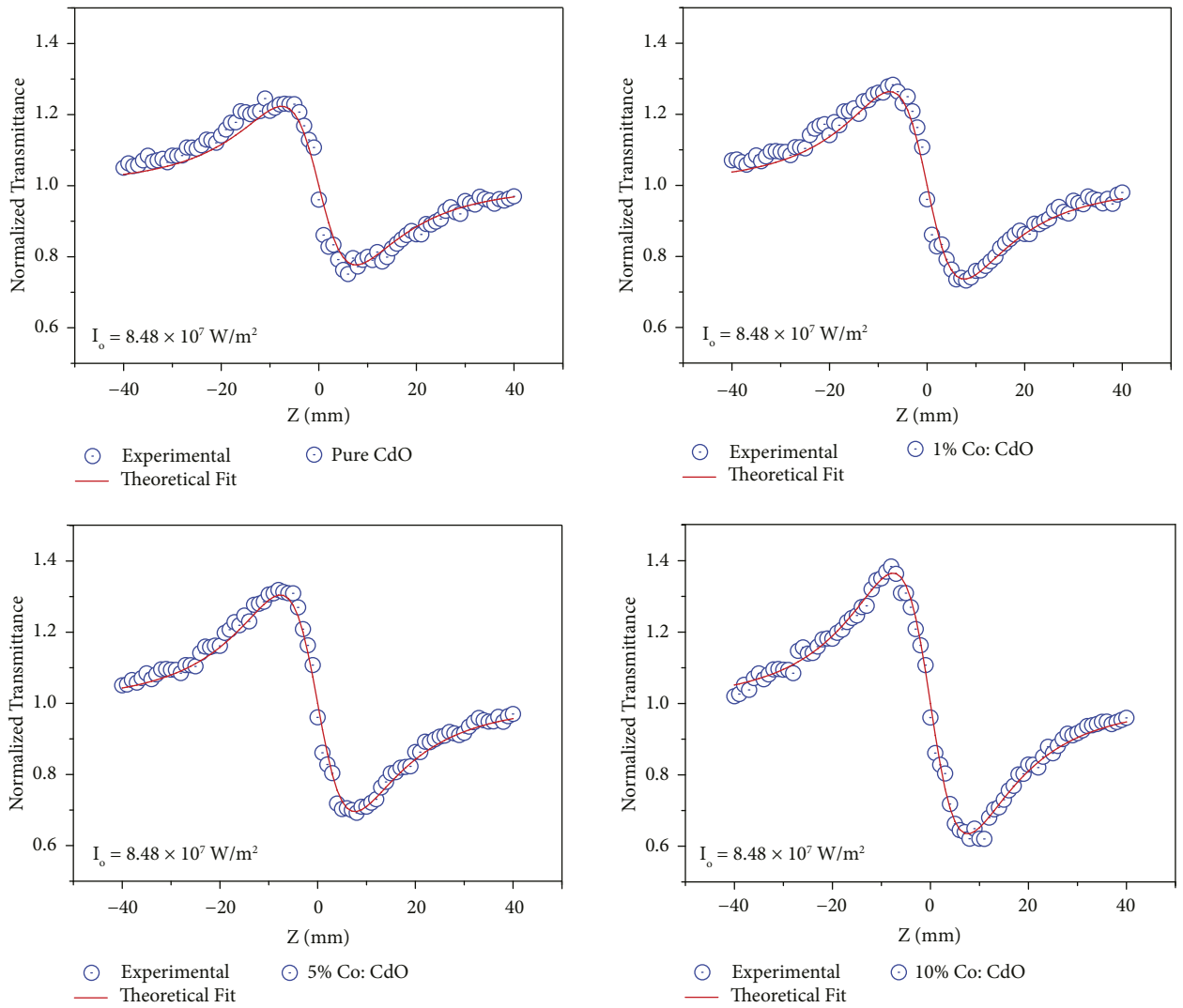

Figure 8: Z-scan CA plots for $Cd_{1-x}Co_xO$ films.

Table 4: Current and reported values of β, n_2 and $\chi^{(3)}$ for some metal oxide films.

Authors	Materials	β (cm/W)	(e.s.u.)	$\chi^{(3)}$ (e.s.u.)
Present work	Co: CdO	1.16×10^{-3}–4.12×10^{-3}	-1.06×10^{-9}–-3.32×10^{-9}	1.23×10^{-4}–5.62×10^{-4}
Bairy et al. [8] (Physica B, 555 (2019) 145–151)	Al: CdO	2.52×10^{-4}–7.25×10^{-4}	-2.01×10^{-9}–-3.92×10^{-9}	3.12×10^{-5}–6.36×10^{-5}
Khan et al. [40] (Journal of Electronic Materials 47 (2018) 5386–5395)	Zn: CdO	------	1.8×10^{-12}–6.1×10^{-10}	0.02×10^{-11}–5.5×10^{-11}
Henari et al. [41] (*Laser Phys.* 18, 1557–1561 (2008))	H: CdO	------	2.4×10^{-14}–5.5×10^{-10}	4×10^{-13}–3.5×10^{-11}
Khan et al. [42] (Journal of Electronic Materials 48 (2019) 1122–1132)	Ag: CdS	------	1×10^{-9}–2×10^{-7}	2.92×10^{-10}–1×10^{-7}

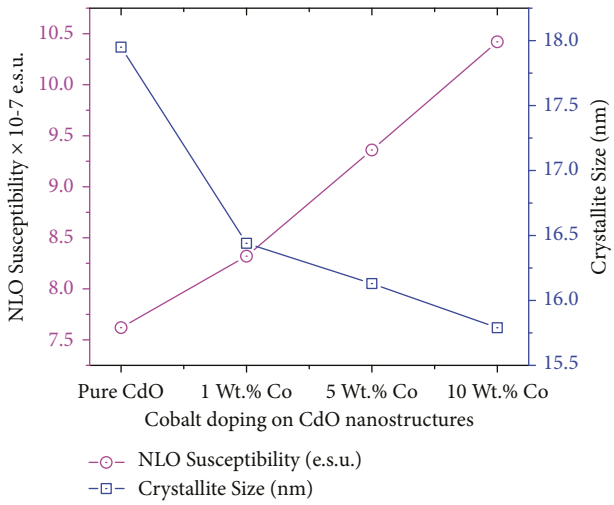

FIGURE 9: Variations of NLO susceptibility (e.s.u.) with crystallite size (nm) for the different Co-doping in the $Cd_{1-x}Co_xO$ thin films.

4. Conclusion

Thin films of Co-doped CdO with different contents of Co were prepared on the glass substrates at 300°C using the SP technique. To understand the structural and morphological changes in the films, XRD and FESEM were studied for each sample. The P-XRD patterns revealed an increase in the crystalline behavior of the sample in preferentially (111) and (200) plane directions strongly. FESEM images revealed the surface morphology of the prepared samples, with spherically shaped grains and smoothening with increased Co-doping content. With the increasing Co-doping, the UV-Visible double–beam spectra confirm the increase of absorption in the visible and UV region. The band gap of the fabricated films decreases by increasing the Co-doping concentration. The third-order NLO studies are carried out using the Z-scan technique, which revealed the TPA in NLO behavior. The value of ⟦ n⟧_2, β, and $\chi^{(3)}$ was enhanced by increasing the Co-doping concentration. These results suggest that the prepared $Cd_{1-x}Co_xO$ thin film samples enriching NLO behavior are more applicable as modulators in optical devices.

Data Availability

No data were used to support this study.

Conflicts of Interest

The authors declare that there are no conflicts of interest.

Acknowledgments

The authors thank N.M.A.M.I.T. NITTE (deemed-to-be-university), Karnataka, India, for providing all research facilities and support for this study.

References

[1] A. J. Freeman, K. R. Poeppelmeier, T. O. Mason, R. P. H. Chang, and T. J. Marks, "Chemical and thin-film strategies for new transparent conducting oxides," *MRS Bulletin*, vol. 25, no. 8, pp. 45–51, 2000.

[2] M. A. Koondhar, I. A. Laghari, B. M. Asfaw, R. Reji Kumar, and A. H. Lenin, "Experimental and simulation-based comparative analysis of different parameters of PV module," *Scientific African*, vol. 16, p. e01197, July 2022.

[3] T. J. Coutts, D. L. Young, X. Li, W. P. Mulligan, and X. Wu, "Search for improved transparent conducting oxides: a fundamental investigation of CdO, Cd2SnO4, and Zn2SnO4," *Journal of Vacuum Science and Technology A*, vol. 18, no. 6, pp. 2646–2660, 2000.

[4] R. Chandiramouli and B. G. Jeyaprakash, "Review of CdO thin films," *Solid State Sciences*, vol. 16, pp. 102–110, 2013.

[5] B. K. Hussein, H. K. Hassun, B. K. Maiyaly, and S. H. Aleabi, "Effect of copper on physical properties of CdO thin films and n-CdO: Cu/p-Si heterojunction," *Journal of Ovonic Research*, vol. 18, no. 1, pp. 37–34, 2022.

[6] A. A. Dakhel, "Study of high mobility carriers in Ni-doped CdO films," *Bulletin of Materials Science*, vol. 36, no. 5, pp. 819–825, 2013.

[7] P. Velusamy, K. Ramamurthi, E. Elamurugu, and J. Viegas, "Study of alloys," *Journal of Alloys and Compounds*, p. 708, 2017.

[8] R. Bairy, S. D. Kulkarni, and M. S. Murari, "Effect of Al doping on photoluminescence and laser stimulated nonlinear optical features of CdO nanostructures for optoelectronic device applications," *Optics & Laser Technology*, vol. 126, Article ID 106113, 2020.

[9] V. Ganesh, M. Shkir, S. Alfaify, I. S. Yahia, and H. Zahran, "Abd el-rehim," *Journal of Molecular Structure*, p. 1150, 2017.

[10] S. Jin, Y. Yang, J. E. Medvedeva et al., "Dopant ion size and electronic structure effects on transparent conducting oxides. Sc-doped CdO thin films grown by MOCVD," *Journal of the American Chemical Society*, vol. 126, no. 42, Article ID 13787, 2004.

[11] A. L. Patterson, "The scherrer formula for X-ray particle size determination," *Physics Reviews*, vol. 56, no. 10, pp. 978–982, 1939.

[12] A. Singh, S. Schipmann, A. Mathur et al., "Structure and morphology of magnetron sputter deposited ultrathin ZnO films on confined polymeric template," *Applied Surface Science*, vol. 414, pp. 114–123, 2017.

[13] H. Shashidharagowda and S. N. Mathad, "Effect of incorporation of copper on structural properties of spinel nickel manganites by co-precipitation method," *Materials Science for Energy Technologies*, vol. 3, no. 9, pp. 201–208, 2020.

[14] M. Benhaliliba, C. Benouis, A. Tiburcio-Silver et al., "Luminescence and physical properties of copper doped CdO derived nanostructures," *Journal of Luminescence*, vol. 132, no. 10, pp. 2653–2658, 2012.

[15] S. Jin, Y. Yang, J. E. Medvedeva et al., "Tuning the properties of transparent oxide conductors. Dopant ion size and electronic structure effects on CdO-based transparent conducting oxides. Ga- and in-doped CdO thin films grown by MOCVD," *Chemistry of Materials*, vol. 20, no. 1, pp. 220–230, 2008.

[16] B. S. Nagaraja, S. C. Gurumurthy, R. Bairy, K. Ramam, K. Bindu, and A. Rao, "Optical materials," *Chemicals*, vol. 122, Article ID 111669, 2021.

[17] S. N. Garaje, S. K. Apte, S. D. Naik et al., "Template-free synthesis of nanostructured $Cd_xZn_{1-x}S$ with tunable band structure for H_2 production and organic dye degradation using solar light," *Environmental Science & Technology*, vol. 47, no. 12, pp. 6664–6672, 2013.

[18] R. Bairy, D. Haleshappa, and M. S. Murari, "The structural, linear and nonlinear optical properties of high-quality Zn1-xPbxO nanostructured thin films for optoelectronic device applications," *Applied Physics B*, vol. 127, no. 8, p. 113, 2021.

[19] M. G. AliBadawi, S. S. Alharthi, and A. M. Al Baradi, "Structure of the paper," *Physics Letters A*, no. 411, pp. 30 2021–127553, 2021.

[20] J. Tauc, *Amorphous and Liquid Semiconductors*, p. 159, Plenum Press, New York, USA, 1974.

[21] I. S. Yahia, G. F. Salem, M. S. Abd El-sadek, and F. Yakuphanoglu, "Optical properties of Al-CdO nanoclusters thin films," *Superlattices and Microstructures*, vol. 64, pp. 178–184, 2013.

[22] J. P. Enriquez and X. Mathew, "Energy of the solution paper," *Solar Energy Materials & Solar Cells*, vol. 76, pp. 313–322, 2003.

[23] T. Sivaraman, V. Narasimman, V. Nagarethinam, and A. Balu, "Effect of chlorine doping on the structural, morphological, optical and electrical properties of spray deposited CdS thin films," *Progress in Natural Science: Materials International*, vol. 25, no. 5, pp. 392–398, 2015.

[24] D. Arivuoli, "Fundamentals of nonlinear optical materials," *Pramana*, vol. 57, no. 5-6, pp. 871–883, 2001.

[25] Z. Chai, X. Hu, F. Wang, X. Niu, J. Xie, and Q. Gong, "Ultrafast all-optical switching," *Advanced Optical Materials*, vol. 5, no. 7, Article ID 1600665, 2016.

[26] M. Frumar, J. Jedelsk, B. Frumarova, T. Wagner, and M. Hrdlĭcka, *Journal of Non-Crystalline Solids*, vol. 326, pp. 399–404, 2003.

[27] M. Sheik-Bahae, A. A. Said, T. H. Wei, D. J. Hagan, and E. W. Van Stryland, *IEEE Journal of*, vol. 26, pp. 760–769, 1990.

[28] R. Bairy, P. S. Patil, S. R. Maidur, H. Vijeth, M. S. Murari, and K. U. Bhat, "The role of cobalt doping in tuning the band gap, surface morphology and third-order optical nonlinearities of ZnO nanostructures for NLO device applications," *RSC Advances*, vol. 9, no. 39, Article ID 22302, 2019.

[29] R. Bairy, A. Jayarama, and M. S. Murari, "Significant effect of film thickness on morphology and third-order optical nonlinearities of Cd1−xZnxO semiconductor nanostructures for optoelectronics," *Applied Physics A*, vol. 126, no. 8, p. 603, 2020.

[30] Q. Bellier, N. S. Makarov, P. A. Bouit et al., "Excited state absorption: a key phenomenon for the improvement of biphotonic based optical limiting at telecommunication wavelengths," *Physical Chemistry Chemical Physics*, vol. 14, no. 44, Article ID 15299, 2012.

[31] T. Jia, T. He, P. Li, Y. Mo, and Y. Cui, "A study of the thermal-induced nonlinearity of Au and Ag colloids prepared by the chemical reaction method," *Optics & Laser Technology*, vol. 40, no. 7, pp. 936–940, 2008.

[32] M. R. Ferdinandus, M. Reichert, T. R. Ensley et al., "Dual-arm Z-scan technique to extract dilute solute nonlinearities from solution measurements," *Optical Materials Express*, vol. 2, no. 12, pp. 1776–1790, 2012.

[33] R. Bairy, S. D. Kulkarni, M. S. Murari, and K. N. Narasimhamurthy, "An investigation of third-order nonlinear optical and limiting properties of spray pyrolysis-deposited Co:CdS nanostructures for optoelectronics," *Applied Physics A*, vol. 126, no. 5, p. 380, 2020.

[34] R. Bairy, A. Jayarama, S. D. Kulkarni, M. S. Murari, and H. Vijeth, "Materials research express," *Solution of matter*, pp. 1–11, 2019.

[35] S. S. Benal, J. V. Tawade, M. M. Biradar, and A. H. Lenin, "Effects of the magnetohydrodynamic flow within the boundary layer of a jeffery fluid in a porous medium over a shrinking/stretching sheet," *Mathematical Problems in Engineering*, vol. 2022, Article ID 7326504, 11 pages, 2022.

[36] M. Ashaduzzman, M. K. R. Khan, A. M. M. Tanveer Karim, and M. Mozibur Rahman, "Influence of chromium on structural, non-linear optical constants and transport properties of CdO thin films," *Surfaces and Interfaces*, vol. 12, pp. 135–144, 2018.

[37] R. Bairy, A. Jayarama, and M. S. Murari, "Structural, linear and nonlinear optical properties of Cd1−xAlxS semiconductor nanostructures: i," *Materials Today Proceedings*, vol. 35, pp. 483–488, 2021.

[38] Z. R. Khan, M. Shkir, M. Shkir et al., "Structural, linear and third order nonlinear optical properties of sol-gel grown Ag-CdS nanocrystalline thin films," *Journal of Electronic Materials*, vol. 48, no. 2, pp. 1122–1132, 2019.

[39] M. A. Manthrammel, M. Shkir, M. Anis, S. S. Shaikh, H. E. Ali, and S. AlFaify, "Facile spray pyrolysis fabrication of Al:CdS thin films and their key linear and third order nonlinear optical analysis for optoelectronic applications," *Optical Materials*, vol. 100, Article ID 109696, 2020.

[40] Z. R. Khan, M. Gandouzi, A. S. Alshammari, M. Bouzidi, and M. Shkir, "The problem faced by the effect," *Journal of elements*, vol. 12, pp. 1–15, 2021.

[41] F. Z. Henari and A. A. Dakhel, "Linear and nonlinear optical properties of hydrogenated CdO thin films," *Laser Physics*, vol. 18, no. 12, pp. 1557–1561, 2008.

[42] Z. R. Khan, M. Munirah, M. Shkir et al., "Structural, linear and third order nonlinear optical properties of sol-gel grown Ag-CdS nanocrystalline thin films," *Journal of Electronic Materials*, vol. 48, no. 2, pp. 1122–1132, 2019.